

AD 750042

**AIR FORCE FLIGHT DYNAMICS LABORATORY
DIRECTOR OF LABORATORIES
AIR FORCE SYSTEMS COMMAND
WRIGHT PATTERSON AIR FORCE BASE OHIO**

**FINAL SCIENTIFIC REPORT
DRAG COEFFICIENTS OF CONES**



May 1972

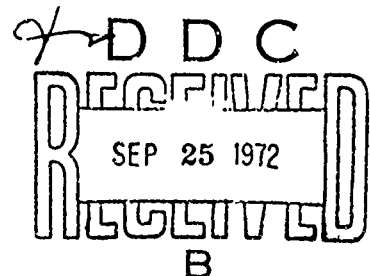
John F. Wendt

von Karman Institute for Fluid Dynamics
Rhode Saint Genese
Belgium

This document has been approved for public release and sale;
its distribution is unlimited.

This research has been sponsored in part by the Air Force Flight
Dynamics Laboratory (FXG), Wright-Patterson AFB, Ohio, 45433
through the European Office of Aerospace Research, OAR, United
States Air Force, under Contract F61052-70-C-0018.

Reproduced by
**NATIONAL TECHNICAL
INFORMATION SERVICE**
U.S. Department of Commerce
NIST A 22151



DOCUMENT CONTROL DATA - R & D

(Security classification of title, body of abstract and indexing annotation must be entered when the overall report is classified)

| | | | |
|---|------------------------|--|--|
| 1. ORIGINATING ACTIVITY (Corporate author) | | 2a. REPORT SECURITY CLASSIFICATION | |
| von Karman Institute for Fluid Dynamics Chaussee de Waterloo, 72 1640 Rhode saint Genese, Belgium | | Unclassified | |
| 3. REPORT TITLE | | 2b. GROUP | |
| Drag coefficient of cones | | | |
| 4. DESCRIPTIVE NOTES (Type of report and inclusive dates) | | | |
| Scientific Final 1 March 1970 - 30 November 1971 | | | |
| 5. AUTHOR(S) (First name, middle initial, last name) | | | |
| Wendt, John F. | | | |
| 6. REPORT DATE | 7a. TOTAL NO. OF PAGES | 7b. NO. OF REFS | |
| | 51 | 15 | |
| 8a. CONTRACT OR GRANT NO. F61052-70-C-0018 | | 9a. ORIGINATOR'S REPORT NUMBER(S) | |
| b. PROJECT NO. AFFDL 1366 | | | |
| c. | | 9b. OTHER REPORT NOT(S) (Any other numbers that may be assigned this report) | |
| d. | | AFFDL TM 72-23 FXG | |
| 10. DISTRIBUTION STATEMENT | | | |
| This document has been approved for public release and sale; its distribution is unlimited. | | | |
| 11. SUPPLEMENTARY NOTES | | 12. SPONSORING MILITARY ACTIVITY | |
| Tech, Other | | Air Force Flight Dynamics Lab. (FXG) Wright Patterson AFB Ohio 45433 | |
| 13. ABSTRACT | | | |
| <p>The objective of this research was to provide experimental values for cone drag coefficients in the near free molecule and transitional flow regimes including an examination of the effects of Mach number, wall speed ratio, bluntness, and specific heat ratio. A modulated force probe with a sensitivity in the microgram range was employed to measure the drag forces on 9° half-angle cones in the range $6 < M_\infty < 10$, $1 < Re_{w, \theta} < 50$ with an RMS dispersion of $\pm 2\%$. A knowledge of the flow properties in the free jet employed for this study permitted the calculation of cone drag coefficients. The resulting values cover the flow regimes from near-free-molecule to transitional.</p> <p>The experimental data are presented as a function of the dimensionless parameters: wall Re number, and free-stream Knudsen number. In addition an "effective" Knudsen number, based on reflected incident molecular collisions employing velocity dependent cross sections is shown, based on limited data, to provide a valid correlation for various values of M number and specific heat ratio as long as cone angle and wall speed ratio are fixed. The relationship between $Kn_{ri,D}$ and the parameters commonly employed in the literature is examined and shown to be consistent in limiting cases.</p> | | | |

1A

1 1 P 4 X A

LINK 14

LINK C

ROLE

W T

ROLL

W I

ROLE

W T

Abstract

[illegible]

Source: *U.S. Census Bureau, 1990*

1

FINAL SCIENTIFIC REPORT

DRAG COEFFICIENTS OF CONES

May 1972

John F. Wendt

von Karman Institute for Fluid Dynamics
Rhode Saint Genese
Belgium

This document has been approved for public release and sale;
its distribution is unlimited.

This research has been sponsored in part by the Air Force Flight
Dynamics Laboratory (FXG), Wright-Patterson AFB, Ohio, 45433
through the European Office of Aerospace Research, OAR, United
States Air Force, under Contract F 61052-70-C-0018.

FOREWORD

This work was supported by the Air Force Flight Dynamics Laboratory (FXG), Wright-Patterson AFB, Ohio under Project number 1366.

The results presented were obtained by the von Karman Institute for Fluid Dynamics, Rhode Saint Genese, Belgium, under Contract F 61052-70-C-0018.

The author wishes to acknowledge the support furnished by a grant from the Mechanics Division of the Air Force Office of Scientific Research which aided materially in the development of the modulated force probe used in this study. In addition, sincere thanks are expressed to Professor Jean J. Smolderen for many stimulating discussions on all facets of this work.

This technical memorandum has been published for exchange of information purposes only.


PHILIP P. ANTONATOS
Chief, Flight Mechanics Division
AF Flight Dynamics Laboratory

ABSTRACT

The objective of this research was to provide experimental values for cone drag coefficients in the near free molecule and transitional flow regimes including an examination of the effects of Mach number, wall speed ratio, bluntness, and specific heat ratio.

A modulated force probe with a sensitivity in the microgram range was employed to measure the drag forces on 9° half-angle cones in the range $6 < M_\infty < 10$, $1 < Re_{w,\ell} < 50$ with an R.M.S. dispersion of $\pm 2\%$. A knowledge of the flow properties in the free jet employed for this study permitted the calculation of cone drag coefficients. The resulting values cover the flow regimes from near-free-molecule to transitional.

The experimental data are presented as a function of the dimensionless parameters: wall Reynolds number, $Re_{w,\ell}$, and free-stream Knudsen number, Kn_∞, D . In addition, an "effective" Knudsen number, $Kn_{ri,D}$, based on reflected-incident molecular collisions employing velocity dependent cross section is shown, based on limited data, to provide a valid correlation for various values of Mach number and specific heat ratio as long as cone angle and wall speed ratio are fixed. The relationship between $Kn_{ri,D}$ and the parameters commonly employed in the literature is examined and shown to be consistent in limiting cases.

TABLE OF CONTENTS

| | |
|--|----|
| FOREWORD | i |
| ABSTRACT | ii |
| LIST OF ILLUSTRATIONS | iv |
| LIST OF ABBREVIATIONS AND SYMBOLS | v |
| 1. INTRODUCTION | 1 |
| 2. DESCRIPTION OF MEASUREMENT TECHNIQUE | 2 |
| 2.1 Principle of operation | 2 |
| 2.2 Calibration of the force probe | 3 |
| 3. FLOW FIELD PROPERTIES | 4 |
| 3.1 The ideal free jet flow field | 4 |
| 3.2 Experimental arrangement | 5 |
| 3.3 Non-ideal free jet flow field | 6 |
| 4. EXPERIMENTAL RESULTS | 10 |
| 5. DISCUSSION OF RESULTS | 16 |
| 6. A CORRELATION PARAMETER FOR CONE DRAG | 19 |
| 7. SUMMARY | 26 |
| REFERENCES | 27 |
| TABLE 1 | 29 |
| TABLE 2 | 31 |

LIST OF ILLUSTRATIONS

| <u>Figure</u> | <u>Title</u> |
|---------------|---|
| 1 | Block diagram of Modulated Flow System |
| 2 | Schematic of Force Probe |
| 3 | Schematic of Calibration Arrangement |
| 4 | Typical Transducer Calibration |
| 5 | Characteristics of Free Jet Expansion for Hypersonic Flow |
| 6 | Schematic of Inconel Heater |
| 7 | Flow Establishment in a Modulated Free Jet |
| 8 | Impact Pressure Variation in Free Jet |
| 9 | Density Variation on Free Jet Centerline Measured with Electron Beam Fluorescence Probe |
| 10 | Dimensionless Cone Drag Coefficient vs Wall Reynolds Number |
| 11 | Dimensionless Cone Drag Coefficient vs Knudsen Number |
| 12 | Dimensionless Cone Drag Coefficient vs Effective Knudsen Number |
| 13 | Dimensionless Cone Drag Coefficient for Various Gases |

LIST OF ABBREVIATIONS AND SYMBOLS

| | |
|------------------|---|
| A_{REF} | Cone base area $\equiv \pi D^2/4$ |
| \vec{c} | Thermal, random or peculiar velocity |
| C_D | Drag coefficient $\equiv F_D / \frac{1}{2} \rho_\infty U_\infty^2 A_{REF}$ |
| D^* | Effective orifice diameter for one-dimensional flow |
| D | Cone base diameter |
| F_{DRAG} | Drag force |
| \vec{g} | Relative molecular velocity |
| Kn | Knudsen number |
| M | Mach Number |
| \dot{m} | Mass flow rate |
| n | Particle density |
| p | Pressure |
| R | Gas constant for a particular gas |
| Re | Reynolds number |
| S_∞ | Free stream speed ratio $\equiv U_\infty / \sqrt{2RT_\infty} = \sqrt{\gamma/2} M_\infty$ |
| S_w | Body speed ratio $\equiv U_\infty / \sqrt{2RT_w}$ |
| t | Time |
| T | Temperature |
| \vec{U}_∞ | Bulk or mean flow velocity |
| x | Axial distance from free-jet orifice |
| α_{bc} | Expansion parameter of Willis (Ref. 1) |
| λ | Mean free path |
| λ_{ri} | Mean free path of "body" molecule with respect to free-stream molecule (reflected wrt incident) |
| ρ | Mass density |
| Σ | Collision cross section $\equiv \pi \sigma^2 \Omega_\mu(T)$ |
| σ | Molecular diameter |
| $\vec{\xi}$ | Molecular velocity $\equiv \vec{U} + \vec{c}$ |
| μ | Viscosity |
| θ_c | Cone half-angle |
| γ | Ratio of specific heats |
| $\Omega_\mu(T)$ | Temperature dependent correction to collision cross section |
| τ | Period of disc rotation |

Subscripts

| | |
|----------|--|
| a | Ambient conditions |
| r | Molecules reflected from the body |
| i | Molecules incident on the body |
| ∞ | Free stream conditions |
| 0 | Stagnation conditions |
| f.m. | Free-molecule conditions |
| w | Conditions on the body (wall) |
| l | Conditions based on cone length |
| D | Conditions based on cone base diameter |
| M | Location of Mach disc |

1. INTRODUCTION

Although considerable progress has been witnessed during the last few years in providing experimental data and theoretical predictions on the drag of slender cones at zero angle of attack in the rarefied hypersonic flow regime, a completely satisfactory understanding of the problem seems still not to be in hand. An excellent critique of near free molecule theories and a discussion of available experimental results have recently been presented by Keel and Willis (Ref. 1). It contains numerous references to earlier studies which will not be repeated here.

The objective of this study was to provide further experimental information on 9° half-angle cones in the Mach number range from 6 to 10 and to assess the effects of specific heat ratio, bluntness, and wall-to-stagnation-temperature ratio (wall speed ratio). A correlation parameter, the Knudsen number characterizing reflected-incident collisions, incorporating temperature-dependent collision cross sections, is introduced and its usefulness is examined by considering selected sets of experimental data from the literature.

2. DESCRIPTION OF MEASUREMENT TECHNIQUE

This section describes the operating principle of the modulated force probe and the calibration procedure employed for these measurements.

2.1 Principle of Operation

Low density wind tunnels seldom are capable of producing reasonably large-scale flow fields with mean-free-paths greater than 5 to 10 mm. Since it may easily be shown that the drag force on a model with dimensions of order millimeters in a hypersonic cold flow at $Kn_{\infty,D} \sim O(10)$ is the order of milligrams, it is clear that a measurement technique suitable for the transitional ($0.3 < Kn_{\infty,D} < 3$) and near free molecule ($3 < Kn_{\infty,D} < 10$) regimes must exhibit a sensitivity of 10 to 100 μ grams to provide a "1%" measurement.

For this purpose, an instrument was developed at the VKI whose operation is based on the principle of flow modulation. Operational details may be found in Reference 2. Briefly, modulating (turning "on" and "off" periodically) the flow acting on a body attached to a typical ceramic force transducer produces an A.C. output whose peak-to-peak amplitude is directly proportional to the applied force. A P.A.R. Model JB-6 lock-in amplifier (a highly tuned amplifier - synchronous demodulator), employing the modulating frequency as a reference, allows the signal of interest to be extracted even when very low values of the signal-to-noise ratio exist. A schematic of the instrument chain is shown in Figure 1.

The flow field in which these drag measurements were performed is a free-jet expansion which provides a high Mach number, low density flow (described in detail in the following chapter) without the attendant problem of boundary layer growth experienced when the more common de Laval geometry is employed. In addition, the small size of the jet orifice allows the flow to be modulated quite easily. A disc with a semi-circular window

is positioned very close to the orifice plane with the result that the flow is periodically turned on and off at its source. A resolver on the disc's shaft then provides the reference signal for the lock-in amplifier. The modulation frequency is 15 Hz.

The probe itself, shown in Figure 2, employs a lead-zirconate-titanate ferroelectric transducer (PZT-5 manufactured by Brush-Clevite) to which the sting and model are rigidly connected. Much of the sting is shielded to reduce the ever-present tare drag.

2.2 Calibration of the Force Probe

The modulated force probe is calibrated by replacing the model with a wire loop and then inserting a straight well-defined segment of this loop into the uniform and known field of a permanent magnet. A precisely measured A.C. current through the wire loop thus produces an accurately known axial force acting on the transducer due to the $\vec{j} \times \vec{B}$ effect. A schematic of the calibration system appears in Figure 3.

When proper attention is paid to ground loops and stray fields, forces as small as 30 μ grams can be measured with a sensitivity of about 1 μ gram. An example of a typical calibration result appears on Figure 4. Note the high degree of linearity over several orders of magnitude of applied force and the small scatter. The probe is calibrated both before and after each series of wind tunnel tests. Naturally, the electronic chain is precisely the same during calibration and wind-tunnel tests. The accuracy of the calibration is estimated to be $\pm 1\%$.

3. FLOW FIELD PROPERTIES

In this section, the "ideal" free jet flow properties are described to present a simple picture of the flow field employed for the force measurements. Then the experimental arrangement is discussed with particular attention to design problems encountered when heated flows are employed. Finally, the real or non-ideal free jet is discussed with the emphasis on problems peculiar to this investigation.

3.1 The Ideal Free Jet Flow Field

The free-jet expansion (a highly underexpanded jet) is employed to produce high Mach number, low density flows. A schematic diagram of the jet structure is shown in the upper half of Figure 5. As it is a nearly spherical expansion, flow gradients are important; however, the use of sufficiently small models circumvents to a large degree this problem.

The case of a jet exhausting isentropically into a vacuum has been studied in Reference 3 and the results quoted are now widely used to determine "ideal" local flow properties in a free-jet flow. The Mach number on the jet centerline may be expressed uniquely in terms of x/D^* , the distance from the orifice to the point in question divided by the effective nozzle diameter for one-dimensional flow, and γ , the specific heat ratio. The Mach number and density ratio are plotted versus x/D^* in the lower part of Figure 5. Thus, the Reynolds number, Re_∞ , (or Knudsen number Kn_∞) at a fixed x/D^* can be altered independently of M_∞ simply by changing the stagnation pressure, p_0 . The test procedure in a free jet is therefore to select M_∞ , which fixes x/D^* ; then perform the desired measurements at this value of x/D^* by varying p_0 which directly varies Re_∞ or Kn_∞ .

3.2 Experimental Arrangement

Two distinct arrangements have been employed to produce the desired flow field depending on whether or not the flow is to be heated.

Cold flows (room temperature) emanate from a 50 liter settling chamber through a sharp-edged nominal 5 mm diameter orifice. The 30 cm diameter chopper disc is positioned such that the plane of the disc is within 0.5 mm from the plane of the orifice. Stagnation pressures are measured with a Texas Instrument Bourdon Tube Gauge with an absolute accuracy of ± 10 microns Hg. Stagnation temperatures are determined with thermocouples and mass flows are measured with precision "ROTA" rotameters.

Heated flows are produced with an inconel heater shown in Figure 6. Two inconel coils, each carrying the gas load, bring d.c. current to and from the one-liter inconel settling chamber which is surrounded by an auxiliary oven. Radiation shielding protects the model/transducer system from excessive radiative heat transfer. Measurements of the stagnation temperature, T_0 , with thermocouples and calculation of T_0 using the sonic flow technique - requiring a knowledge of the effective orifice diameter D^* , stagnation pressure, p_0 , and mass flow \dot{m} - were in agreement over a wide range of operating conditions. Temperatures up to 1000°K can easily be produced and higher temperatures are certainly possible if and when desired, although the radiant heat transfer losses then become significant.

In each of the above cases, the force probe and support are mounted on a platform suspended by rubber supports which in turn is attached to a linear-bearing traversing mechanism. Model-orifice alignment is carried out using optical techniques. The model can be positioned with respect to the orifice with an accuracy of 0.2 mm.

3.3 Non-Ideal Free Jet Flow Field

The flow properties in a free jet do not always correspond to the "ideal" picture presented above. This section discusses the practical case of a "non-ideal" free jet.

There are two classes of non-ideal free jet flows which need to be considered: those which are due to the manner in which the free jet is employed in this particular study (primarily resulting from flow modulation), and those which are always observed when free jets at low densities are employed for aerodynamic testing purposes.

Looking at the first class, it is clear that modulating a free jet with a rotating chopper disc produces a periodic partial blockage of the flow which in turn causes the stagnation pressure to rise and fall. Thus, the model will be subjected to a time-varying force when the orifice is uncovered and covered. This problem is easily circumvented by employing a sufficiently large stagnation chamber such that the response time is much greater than the disc's half-period. In cold flow studies, a 50 liter settling chamber is employed which results in pressure fluctuations of a few tenths of one percent. The use of heated flows precludes such a large volume because of the heating requirements that would be imposed. Pressure fluctuations in the one liter settling chamber used for hot flows were reduced to less than 1% by positioning the chopper disc a few millimeters downstream of the orifice plane. Flow effects felt on the free jet centerline due to spillage around the disc during the "flow-off" period were investigated with impact probes and found to be entirely negligible.

Flow transients must also be expected when using a chopper disc. Their form and duration have been studied experimentally with a hot-wire system. When the flow is modulated, the typical response of a nominal one micron wire is that shown on Figure 7. The peaks correspond to the "closing" of the ori-

fice by the rotating disk and appear to be quite clean and sharp. The valleys, on the other hand, correspond to the "opening" of the orifice and are characterized by a small irregularity which is typically 2-3% of the half-period. It is properly termed the flow-establishment time. Note that the "uncovering-time" of the orifice is approximately 1% of the half-period (0.5 cm dia. orifice/50 cm half-circumference of the rotating disk). Thus, the flow transient is, as might be expected, somewhat in excess of the time required to uncover the orifice. However, the ultimate effect of this transient on the force measurements is diminished considerably by the manner in which the lock-in amplifier treats such transients (see Reference 2 for details; basically, the error due to a transient of duration Δt is not $\Delta t/\tau$, where τ is the period of rotation, but rather $(\Delta t/\tau)^2$).

Looking at the second class of problems, it is seen that when using the results of the method of characteristics (Ref. 3) to determine the flow field properties, the effective orifice diameter, D^* , for one dimensional flow must be known. It is nearly, but not precisely, equal to the geometric diameter. For each orifice employed, the effective orifice diameter was calculated as a function of the Reynolds number by measuring the mass flow as a function of stagnation pressure. For all sharp-edged orifices analyzed to date, the effective diameter was found to be only a few percent smaller than the geometric diameter and, more importantly, to vary by no more than two percent over the entire range of source Reynolds numbers employed in the eventual test program. For purposes of computing flow properties, D^* was assumed constant.

A check on the applicability of the method-of-characteristics solution to the free jet was made by measuring the impact pressure along the centerline of the free jet as a function of x/D^* and comparing the measured values with the predicted results. Both heated and unheated flows were employed. The raw experimental points are shown in Figure 6. Corrections

for shock stand-off distance will shift all the data points to the left by about $0.4 x/D^*$. Viscous corrections to the impact pressure measurements are negligible for the unheated cases, but they will shift downwards the data points taken under heated conditions by as much as 6-8 % (Ref. 4) at an x/D^* of $\sqrt{12}$. These considerations, combined with the computed measurement accuracy - about $\pm 1\%$ at an x/D^* of 5 and $\pm 8\%$ at an x/D^* of 12 - allow us to conclude that the impact pressure surveys are in good agreement with theory. They also lend credence to the fact that the flow is not disturbed by either the rotating disk or the radiation shields.

A final non-ideal free jet characteristic is the thickening of the shock waves which form the "barrel" causing the boundaries to encroach on the useful testing region. Electron beam measurements of the free-jet density profiles on the jet centerline have been carried out for different values of the stagnation pressure. The results are shown in Figure 9. The empirical high-density location of the Mach disk $(x_m/D^*)_{th}$ which terminates the hypersonic flow field is calculated from the expression (Ref. 3)

$$\left(\frac{x_m}{D^*}\right)_{th} = \left(\frac{p_0}{p_a}\right)^{1/2} \quad (3-1)$$

It is clearly seen that reducing p_0 , so as to increase λ_∞ , can only be continued to a certain level, depending on the axial location of the model. Below this level, the free jet density profile no longer agrees with the method of characteristics' predictions. The results presented herein all were obtained at values of p_0 such that the measured values of density agree with the theoretical predictions. Therefore, no changes in flow properties occur due to the encroachment of the surrounding shock structure as p_0 is decreased (so as to increase Kn_∞).

In summary, satisfactory operating conditions for the proper use of a free jet flow field have been confirmed by a variety of experimental checks. Within the boundaries specified,

the theoretical values for the free jet flow properties may be used with confidence for data reduction in both cold and hot flows, requiring only a knowledge of the distance from the orifice to the model and the effective diameter of the orifice.

4. EXPERIMENTAL RESULTS

This section describes the test procedure and the results of force measurements on the 9° half-angle cones.

A. Test Procedure

The modulated force probe was fitted with a 0.4 mm diameter sting which supported the cone model in the manner shown on Figure 2. The orifice, from which the free jet emanated, had an effective diameter, D^* , of 5.4 mm. Based on the desired Mach number, the corresponding axial distance from the orifice to the cone was calculated according to the free jet theory discussed earlier (Ref. 3). The sting was optically aligned parallel to the flow centerline as determined by the plane of the orifice.

After stabilizing the wind tunnel flow and the electronic chain, the stagnation pressure was systematically varied over a range from roughly 1-50 Torr and, at each value, the force was measured. Near the above limits, the ambient pressure was increased by $\approx 25\%$ to examine its effect on the readings; if any effect was noted, the reading was discarded as having been influenced by the surrounding shock structure.

When measurements of the force acting on the cone-sting combination were completed, the cone was removed from the sting and suspended by a fine support wire just in front of the sting, providing the proper geometry for a tare measurement; i.e., a measurement of the sting drag alone.

A calibration was performed before and after each wind tunnel series. If the two calibration factors differed by more than 2%, the data were discarded. If less, the average value was chosen for data reduction purposes.

B. Results in Unheated Flows

The force measurements at a given p_0 are normalized by the appropriate free stream properties, computed from a knowledge of model position, x/D^* , and p_0 , to form the desired dimensionless grouping - the cone drag coefficient :

$$C_D = \frac{F_{\text{DRAG}}}{\frac{1}{2} \rho U_{\infty}^2 A_{\text{REF}}} \quad 4-1$$

where $A_{\text{REF}} = \pi D^2/4$. The distance x , is taken as the distance from the orifice to the "half-area" point of the cone; i.e., the point at which half the cone area lies upstream and half downstream, excluding the base area.

The results are shown in Figure 10 for different Mach numbers as a function of the wall Reynolds number,

$$Re_{w,\ell} = \frac{\rho_{\infty} U_{\infty} \ell}{\mu_w} \quad \text{The data are tabulated in Table 1 and the symbols}$$

are identified in Table 2. The accuracy of the data was computed based on the following considerations :

$$\frac{\delta C_D}{C_D} = \frac{\delta F}{F} + \frac{\delta \frac{1}{2} \rho U_{\infty}^2}{\frac{1}{2} \rho U_{\infty}^2} + \frac{\delta A_{\text{REF}}}{A_{\text{REF}}} \quad 4-2$$

In a free jet,

$$\frac{\delta \frac{1}{2} \rho U_{\infty}^2}{\frac{1}{2} \rho U_{\infty}^2} = \frac{\delta p_0}{p_0} + \frac{2\delta x/D}{x/D} \quad 4-3$$

A best estimate of the random error is tabulated below :

| M_∞ | ~ 6 | ~ 8 | ~ 10 |
|-----------------------------|--------------------------|--------------------------|--------------------------|
| Force | $\pm 1.0\%$ | $\pm 1.0\%$ | $\pm 1.0\%$ |
| p_0 | $\pm 1.0\% - \pm 0.05\%$ | $\pm 0.2\% - \pm 0.04\%$ | $\pm 0.2\% - \pm 0.04\%$ |
| x | $\pm 0.5\%$ | $\pm 0.4\%$ | $\pm 0.2\%$ |
| D^* | $\pm 0.5\%$ | $\pm 0.5\%$ | $\pm 0.5\%$ |
| A_{REF} | $\pm 1.0\%$ | $\pm 1.0\%$ | $\pm 1.0\%$ |
| R.M.S. Random Error * | $\pm 2.2\% - \pm 2.0\%$ | $\pm 1.9\%$ | $\pm 1.8\%$ |

Thus a random error of approximately $\pm 2\%$ in C_D can be expected. Naturally, the presence of systematic errors is also possible. In particular, the Mach 6 data appear to be low by roughly 15%; this point is discussed in a later section.

The data presented in Fig. 10, recorded in an unheated flow, include the effects of half-angle, θ_c ; type of gas, γ ; and Mach number, M_∞ . A qualitative test on the effect of bluntness was carried out at Mach 10.4 with two cones having bluntness ratios $R_N/R_B \leq 0.04$ and 0.30. When plotted versus $Re_{w,\ell}$, for example, the blunt cone exhibited slightly lower ($\approx 5\%$) values of C_D than did the sharp cone.

C. Results in Heated Flows

As tests in a heated flow were expected to raise the overall temperature level of the force probe by a not-insignificant amount, calculations were first performed to estimate

* The larger value applies to the lowest value of p_0 (and thus the lowest $Re_{w,\ell}$), the smaller value applies to the largest value of p_0 (and thus the highest $Re_{w,\ell}$).

the equilibrium temperature of the cone model under a variety of flow conditions. Factors included in the calculation were : radiation heat transfer from the interior, exterior and surrounding shields of the settling chamber; convective heat transfer; and conduction heat transfer through the connecting sting and support assembly. Detailed results can be found elsewhere (Ref. 5). Of essential interest was the fact that model temperatures between 350-550°K might be expected with the existing probe design for the anticipated range of flow conditions and a stagnation temperature of 1200°K - the maximum design temperature for the heated stagnation chamber discussed earlier. Considering the specific geometry of the force probe, it was further concluded that the transducer temperature would be about 330°K ($\sim 50^{\circ}\text{C}$). This is well below the Curie temperature of the PZT-5 ferroelectric employed, but it is known that the properties of these crystals are somewhat dependent on temperature over such a range.

A calibration of the transducer was therefore performed in a temperature-controlled oven at temperatures up to 360°K. Small ($\sim 10\%$) changes in the calibration factor of the ferroelectric device were noted, but the performance was otherwise quite stable and repeatable.

When tests in a heated flow in the wind tunnel were initiated, however, completely different results were obtained characterized by marked instabilities and force values which were far removed (15%-25%) from the expected values. Measurements of the model temperature confirmed the earlier predicted values and hence the transducer temperature was certainly well within the limits reached in the oven during calibration (i.e., $<360^{\circ}\text{K}$). The only essential difference between the oven calibration tests and the wind tunnel experiments was that in the latter a temperature gradient existed along the length of the transducer (a ΔT of approximately 10°C), whereas the former were performed at a uniform element temperature.

Since it was desirable to further reduce the model temperature to provide an increased ratio of T_0/T_w , and as such a change would also decrease both ΔT across the transducer as well as the average temperature of the transducer, the probe was modified to provide an alternate conduction path for the heat which would reduce the model and transducer temperature levels at the expense of only a small loss in sensitivity. The result was unsuccessful in the sense that the same unstable operation was observed.

Finally, a special test set-up was arranged to quantitatively examine the effect. In the calibration mode, the supports fore and aft of the transducer (see Fig. 3) were fitted with thermocouples and a blackened foil was cemented with conducting glue to the sting. The light from a 150 watt reflector lamp was focused onto the black foil. Thus, sufficient heat was added forward of the transducer to produce a ΔT across the transducer which could reach 30°C . At the same time, a force could be applied to the element and thus the effect of a well-defined temperature gradient on the output signal could be accurately determined. An oscilloscope provided a direct recording of the signal at the input to the lock-in amplifier. The results were striking. A heat pulse, producing an initial rate of change of ΔT on the order of $0.1^\circ\text{C}/\text{sec}$, caused the transducer output to surge in such a way as to saturate the charge amplifier and momentarily cut to zero the input signal to the lock-in amplifier. Some tens of seconds were required for the system to return to normal operation. Various tests eventually proved conclusively that the responsible cause was the change in element temperature with time. The mechanism is probably a little-understood (from the quantitative point of view) phenomena called the pyro-electric effect. It should be emphasized that the pyro-electric effect can easily produce volts, whereas the largest output signals observed in force measurements are typically millivolts. Thus, complete saturation is quite understandable.

When a time-independent ΔT of 2°C was established across the element, the output signal was quite satisfactory. At a ΔT of 4°C , some unstable operation was noted; enough to remove the element from the realm of a $\pm 1\%$ instrument. At larger ΔT 's, operation was impossible due to large drifts and instabilities.

Since the applied force during all of the above tests was relatively large compared to the values recorded under near-free molecule flow conditions, it became clear that even a $\Delta T = 2^{\circ}\text{C}$ could not be tolerated.

In summary, the heated flow tests could not be carried out with any reasonable degree of accuracy ($< 20\%$) because of a highly unstable output signal produced by a temperature gradient of only a few degrees Celsius or more, a gradient so small that any modifications to the probe design for the purpose of providing increased cooling would have to be so important as to produce unacceptable side-effects; i.e., a highly reduced sensitivity due to the mechanical constraint of the heat-conduction member.

5. DISCUSSION OF RESULTS

An examination of Figure 10 discloses a number of points which are commented on here.

1. The Mach 8.1 data ($\times, +$), while exhibiting little scatter within each set, show a systematic difference from each other which varies from 6 to 8%. A similar result is noted for the Mach 10.4 data (\square, \blacksquare). In principle, the data for each Mach number should be averaged resulting in the conclusion that for these two sets of tests the reproducibility is roughly ± 3 to 4%. As the tare correction typically amounted to 30 - 40% of the total drag, some discrepancy may be due to the inevitable subtraction errors that occur in a sting-mounted arrangement. A second source of error is in the location of the model relative to the orifice. Because of the expanding nature of the flow, the Mach number, and hence normalized dynamic pressure and C_D changes with x/D^* . As an example, an error in x of $\sqrt[1]{2}$ mm will result in a 2 - 3% error in the calculated value of C_D for the Mach 8 case.

2. While the bulk of the data falls on a straight line emanating from the $C_D/C_{D_{f.m.}} = 1$ point, a tendency is noted for the data to rise above this line for $Re_{w,l} < 2$ or 3. This fact has been noted previously (Ref.1, p.33), but whether the effect is real or simply represents experimental difficulties in the regime of very low force levels is not clear.

3. The data have been compared with the predictions of Willis' Knudsen iteration analysis (Ref.1) which provides a first order correction to the free molecule drag coefficient and is based on the modified Krook model for the collision term in the Boltzmannequation. The expansion parameter in Willis' analysis, essentially a Knudsen number, can be defined in different ways depending on the test conditions. Briefly, Willis predicts

$$\frac{C_D - C_{D_{f.m.}}}{C_{D_{f.m.}}} = A \alpha_{bc} \quad 5-1$$

where A is a function of cone angle θ_c , and wall speed ratio, S_w , and α_{bc} is taken to be

$$\alpha_{bc} = \frac{S_w}{2\sqrt{2} \sin \theta_c \text{Kn}(D)} \quad 5-2$$

$$\text{where } \text{Kn}(D) = \frac{\lambda_0 \rho_0}{D \rho_\infty}$$

When these quantities are rewritten in terms of $Re_{w,l}$, the straight lines on Figure 10 result.

It is noted that the agreement between theory and experiment is very good for the $\theta_c = 13.5^\circ$ case and reasonably good for the $\theta_c = 9^\circ$ case (with the exception of the Mach 6 case discussed below), particularly when slopes rather than absolute values are considered.

4. The Mach 6 data are appreciably below ($\approx 15\%$) the other data. While some Mach number effect is anticipated, such a discrepancy is too large to be expected. Noting that a straight line through the Mach 6 data is nearly parallel to the theoretical line (the solid line for $\theta_c = 9^\circ$), it is possible that a systematic error occurred. Extrapolating the data to $Re_{w,l} = 0$ yields a $C_D/C_{D_{f.m.}} = 0.86$ instead of unity. If the values of the ordinates are raised by a corresponding amount, then the "corrected" data for the Mach 6 case will (naturally) fall on or around the solid line and at the same time will agree with the other data. Clearly, no firm theoretical or experimental justification exists for this type of data manipulation. Such a large systematic error could, however, arise due to an error in the measurement of x , the distance from the orifice to the model. In this case, an error of 1.5 mm would be necessary to explain the observed discrepancy. A more likely explanation is related to the

fundamental question regarding the selection of x itself. Is it the distance to the apex, the mid point, the "half-area" point (used herein), or the base? As the models have a nominal length of 5 mm, it is readily seen that the normalized dynamic pressure (and hence the calculated C_D) will vary by $\approx 45\%$ from apex to base for the Mach 6 case because the distance from orifice to apex is 21.4 mm and $\frac{\delta C_D}{C_D} \sim 2 \frac{\delta x}{x}$. (The variation of the normalized dynamic pressure for the Mach 8 to 10 cases is, of course, much less because x is larger; the corresponding percentages would be $\approx 25\%$ and $\approx 15\%$ respectively.) As it is quite difficult to accurately machine smooth slender cone models with a length of less than 5 mm, and as the absolute size of the VKI free jet is quite large compared with others currently in use for similar studies, the wide variation in calculated values of C_D which are possible depending on the choice of x should be kept in mind when analyzing free jet results. In summary, although an evaluation of flow properties at the "half-area" point appears logical, it cannot be said to be correct in an absolute sense.

6. A CORRELATION PARAMETER FOR CONE DRAG

It is clearly of interest to develop a parameter which would correlate cone drag coefficients over a wide range of conditions. In the past, experimentalists in the low density field generally employed the free stream Knudsen number Kn_∞ , while members of the continuum school used the free stream Reynolds number, Re_∞ . Ignoring the effect of relative velocity on collision frequency, the two quantities are related in a simple way as first shown by von Karman; $Kn_\infty \sim M_\infty/Re_\infty$ where the coefficient is of order unity. Thus the two parameters are not at all independent, but on the other hand the success of either one is limited as can be seen in Figure 11, for example, where a wide variety of data has been plotted as a function of $Kn_{\infty,D}^*$. It should not be surprising that Kn_∞ (or Re_∞) is unsuccessful in the low density regime because it says nothing about the effect of the body or wall temperature; an effect which is clearly important in the free molecule regime and thus one which must persist at least to some extent as Kn_∞ decreases.

However, there is general agreement that a Knudsen number based on the mean free path of a molecule leaving the body in question and colliding with an incident or free stream molecule (defined here as λ_{ri}) must characterize the near-free molecule regime. It is a Knudsen number which accounts for both the free stream properties (M_∞, T_∞) and the properties of the wall (T_w) and may, in addition, account for the temperature (or velocity) dependence of the cross section characterizing this particular type of collision. The latter point seems important to this author when comparing results in which the relative

$$* \quad Kn_{\infty,D} \equiv \frac{\lambda_\infty}{D} = \frac{1}{n_\infty \pi \sigma^2 \Omega(T_\infty) D}$$

where $\Omega(T_\infty)$ may be calculated from tables presented in Ref.6.

velocities characterizing collisions in the various wind tunnel experiments on record vary by nearly one order of magnitude. Such a Knudsen number has been successful in correlating a wide variety of sphere drag data (Ref.7).

The purpose of this section, then, is to define a Knudsen number based on a reflected-incident collision process which includes a realistic temperature (or energy) dependent cross section and then to use this so-called "effective" Knudsen number to correlate a variety of cone drag results and assess the consequences. This section essentially repeats material previously presented in Ref.7.

The definition of the "effective" Knudsen number and the definition of the mean free path associated with the collision process is :

$$Kn_{ri,D} = \frac{\lambda_{ri}}{D} = \frac{|\vec{\xi}_r|}{n_{\infty} \Sigma(|\vec{c}_{ri}|) \left| (\vec{\xi}_i - \vec{\xi}_r) \right| D} \quad 6-1$$

$$\text{where } |\vec{c}_{ri}| \equiv |(\vec{\xi}_i - \vec{\xi}_r)|.$$

Since a near-free molecule analysis indicates that the first order correction to the free molecule drag coefficient (see, e.g., Ref.8) goes as :

$$C_{D_{f.m.}} - C_D \sim \frac{1}{Kn_{ri}}$$

therefore

$$\frac{C_D}{C_{D_{f.m.}}} \sim 1 - \frac{1}{C_{D_{f.m.}} Kn_{ri}} \quad 6-2$$

This point is emphasized because it is common (and indeed essential) to normalize near free molecule drag by the free molecule drag coefficient and thus the relevant correlation parameter is more correctly $C_{Df,m.} Kn_{ri}$ rather than just Kn_{ri} . (Since $C_{Df,m.}$ seldom exceeds 3, and then only at low supersonic conditions, and cannot be less than 2, the inclusion of this parameter as a multiplying factor does not exert an important influence on the results).

It remains to put equations 6-1 into a form which will allow the insertion of experimentally measurable quantities. Assume that we can write :

$$\overline{(\vec{\xi}_i - \vec{\xi}_r)^2} = \overline{|\vec{\xi}_i - \vec{\xi}_r|^2}$$

Choosing the x-direction parallel to the bulk velocity U_∞ ; putting the cone at the origin of the coordinate system so that molecules reflected from it have no bulk velocity, but only their random thermal velocity, so that $\vec{\xi}_r \equiv \vec{C}_r$; and using the fact that $\vec{C}_\infty = 0$; we have

$$\overline{(\vec{\xi}_i - \vec{\xi}_r)^2} = U_\infty^2 + 2U_\infty \overline{C_{rx}} + \overline{C_\infty^2} + \overline{C_r^2}$$

Ignoring the complicating effects of geometry and simply picturing all molecules as emanating from a plane perpendicular to the free stream velocity,

$$\overline{C_{rx}} = \frac{\overline{C_r}}{\sqrt{4\pi}} = \sqrt{\frac{RT_w}{2\pi}}$$

(It is clear that this assumption is less adequate for cones than for blunt bodies; however the quality of experimental data to date probably does not justify additional rigor.)

Recalling that $\overline{C^2} = 3RT$, the main term of interest in 6-1 becomes

$$\frac{|\vec{\xi}_r|}{|(\vec{\xi}_i - \vec{\xi}_r)|} = \frac{1}{\sqrt{(S_w^2 \left[\frac{2}{3} + \frac{1}{S_\infty^2} \right] + \frac{2}{3} \frac{S_w}{\sqrt{\pi}} + 1)}} \quad 6-4$$

(Note that for $S_\infty \gg 1$, $S_w \gg 1$; 6-4 is nearly S_w^{-1}).

We define

$$F(S_w, S_\infty) \equiv S_w^2 \left[\frac{2}{3} + \frac{1}{S_\infty^2} \right] + \frac{2}{3} \frac{S_w}{\sqrt{\pi}} + 1 \quad 6-5$$

Therefore,

$$K_{r_i, D} \equiv \frac{\lambda_{ri}}{D} = \frac{1}{n_\infty \Sigma(\overline{r_{ri}})_D \sqrt{F(S_w, S_\infty)}} \quad 6-6$$

The velocity dependent cross section $\Sigma(\overline{r_{ri}})$ must now be put into a sensible form. We compute an equivalent temperature characterizing the collision process by computing the temperature of an equilibrium gas in which the mean square relative velocity between two molecules is taken equal to the mean square relative velocity of a free stream molecule with respect to a molecule emitted from the surface; i.e. in a general equilibrium case :

$$\overline{g^2} \equiv \overline{\vec{C}_1^2} + \overline{\vec{C}_2^2} = 2(3RT_{eq})$$

In the situation described here,

$$\overline{(\vec{\xi}_i - \vec{C}_r)^2} = U_\infty^2 + 2U_\infty C_{rx} + \overline{C_\infty^2} + \overline{C_r^2},$$

which is the mean square relative velocity for the collision geometry considered. Equating the two allows one to define an equivalent temperature for the collision process which is defined in turn as T_{ri} and is given by :

$$T_{eq} \equiv T_{ri} = \frac{1}{2} T_w F(S_w, S_\infty) \quad 6-7$$

where $F(S_w, S_\infty)$ was defined in 6-6.

Note that, as expected, when $S_w \gg 1$ and $S_\infty \gg 1$ (cold wall hypersonic case),

$$T_{ri} \approx \frac{1}{3} \frac{\gamma}{\gamma - 1} T_0 \approx T_0$$

Thus, the effective Knudsen number characterizing collisions between free stream molecules and molecules emanating from a plane at a temperature T_w placed perpendicular to the flow direction may be computed from equations 6-6 and 6-5 where the cross-section is computed at the temperature T_{ri} given by equation 6-7.

It is instructive to note the relationship between Kn_{ri} and parameters employed by other investigators. A few such comparisons follow.

I. Consider the case : $S_w \gg 1$, $S_\infty \geq S_w$ (the hypersonic cold-wall case). From equation 6-5, $F(S_\infty, S_w) \rightarrow S_w^2$ and $T_{ri} \rightarrow T_0$. Then

$$Kn_{ri,D} \approx \frac{1}{n_\infty \Sigma(T_0) D S_w} \approx \frac{Kn_\infty \Sigma(T_\infty)}{S_w \Sigma(T_0)}$$

If $\Sigma = \text{constant}$ (hard sphere case), then $Kn_{ri,D} \sim \frac{Kn_\infty}{S_w}$, a parameter used in Ref. 1, for example.

If $\Sigma \sim T^{-1/2}$ (implying $\mu \sim T$; thus, a "Krook" gas), then

$$Kn_{ri,D} \sim \frac{Kn_\infty S_\infty}{S_w}$$

Since $\mu \sim T^{1/2}/\Sigma(T)$, then using the fact that $Kn \sim M/Re$,

it is seen that $Kn_{ri,D} \sim \frac{1}{Re_0} \sqrt{\frac{T_w}{T_0}}$, the correlation employed in Ref.9.

II. Next, consider the case : $S_w \sim 1$ (the hypersonic hot wall case). From equation 6-5, $F(S_w, S_\infty) \rightarrow 1$ as long as $S_\infty \geq S_w$ and $T_{ri} \rightarrow T_w \approx T_0$ when $S_\infty \gg 1$. Then

$$Kn_{ri,D} \approx \frac{1}{n_\infty \Sigma(T_w) D} \approx Kn_\infty \frac{\Sigma(T_\infty)}{\Sigma(T_w)}$$

If $\Sigma = \text{constant}$, then $Kn_{ri,D} \approx Kn_\infty$.

If $\Sigma \sim T^{-1/2}$, then $Kn_{ri,D} \sim Kn_\infty \sqrt{\frac{T_w}{T_\infty}}$; but since $T_w \approx T_0$ when $S_w \sim 1$ if $S_\infty \gg 1$, it follows that $Kn_{ri,D} \sim Kn_\infty M_\infty$. Thus, it is readily seen that the effective correlation parameter for this problem, restricting our attention to the hypersonic case, may be expressed as the product of Kn_∞ and a quantity which will vary from $1/S_w$ to S_∞/S_w to 1 to S_∞ depending on the temperature dependence of the collision cross section and the relative magnitude of S_w compared to unity.

It is seen that the effective Knudsen number defined in 6-1 reduces to the conventional forms of Kn (or Re) under certain limiting conditions. Therefore, it is clear that a realistic temperature-dependent cross section must be incorporated in any such correlation parameter if a wide variety of data representing many distinctly different flow conditions are to be adequately correlated.

A limited amount of slender sharp cone drag data has been plotted in terms of $Kn_{ri,D} C_{Df.m.}$ on Figure 12. The symbols are defined in Table 2. The wall speed ratios vary from 1.5 to 10, γ from 1.30 (CO_2) to 1.67(A), M_∞ from 3.7 to 24, and θ_c from 6° to 15° .

A word of caution must be expressed (and possibly an apology as well) regarding the translation of data, originally expressed in terms of Kn_∞ , Re_w , etc., into $Kn_{ri,D}$. In some cases, a bit of guessing as to the values of unspecified flow or model conditions was required to effect the transformation. In other cases, certain flow conditions were recomputed; e.g., Geiger's values of Re_∞ in Ref.10 were recalculated because the Sutherland viscosity law used therein is well known to be incorrect at values of T_∞ below 50°K. The Chapman-Enskog viscosity with temperature-dependent cross sections (Ref.6) was employed in all data manipulation for consistency. In addition, the data of Kussoy et al (Ref.12) was actually taken from the graphs of Ref.1.

The results in Figure 12 are not as strikingly clear as in Ref.7 for sphere drag where much more data were available. In that case, it was found that data for different γ 's and M_∞ 's fell on a single curve for a given value of S_w and that as S_w increased, $C_D/C_{Df.m.}$ increased for a fixed value of $Kn_{ri,D}$. Here the same trend can be inferred only if Geiger's data are ignored. It should be mentioned that Willis' theoretical predictions (Ref.1) lie above Geiger's results, below the results of Jones and Miller (Ref.11), and generally somewhat below the results of Kussoy, et al. (Ref.12). Willis' theory also predicts the same variation of $C_D/C_{Df.m.}$ with S_w as suggested here.

A close inspection of Figure 12 illustrates that the quantity $Kn_{ri,D} C_{Df.m.}$ is a useful correlation parameter. This assertion is borne out when three sets of data for nearly the same S_w are plotted in Figure 13. Note that although γ varies from 1.3 to 1.67 and M_∞ varies from 3.7 to 11.5, a satisfactory correlation is achieved. It might even be argued that the CO₂ data of Sims (Ref.13) would be expected to lie somewhat above the other data because the cone half-angle in Sims' case is somewhat smaller (10°) than the other cases (13.5°) - again a trend predicted by Willis' theory.

7. SUMMARY

Drag coefficients for sharp 9° cones have been experimentally determined in the hypersonic hot-wall regime at nominal Mach numbers of 6, 8 and 10. The results are in satisfactory agreement with the data of other investigators and with Willis' theory for the near-free molecule regime. Cones with a bluntness ratio of 0.3 exhibit slightly smaller values of C_D at otherwise identical conditions.

The correlation parameter Kn_{ri} , successfully employed for blunt bodies, appears to correlate data in the transitional and near-free molecule regimes for varying Mach numbers and specific heat ratios if the wall speed ratio is constant.

More precise data on slender cones are required in the cold-wall regime before a more definitive statement can be made regarding the adequacy and limits of applicability of this parameter.

REFERENCES






1. Keel, A.G., Jr. and Willis, D.R., "Critique of Near-Free Molecule Theories for Flow over Cones", University of California Report AS-71-5, July 1971.
2. Smolderen, J.J. and Wendt, J.F., "The Measurement of Drag Forces in Low Density Flows using a Modulation Technique", Proc. 18th Int. Astron. Congress, Pergamon Press, 1968. (also VKI TN 44).
3. Ashkenas, H. and Sherman, F.S., "The Structure and Utilization of Supersonic Free Jets in Low Density Wind Tunnels", Rarefied Gas Dynamics, Ed. by J.H. de Leeuw, Academic Press, New York, 1966, Vol. II, pp. 84-105.
4. Bailey, A.B. and Boylan, D.E., "Some Experiments on Impact Pressure Probes in a Low-Density, Hypervelocity Flow", AEDC-TN-61-161, December 1961.
5. Dinraths, J.P., "Design Study of a Heater for a Low Density Hypersonic Air Flow", VKI-PR 69-233, June 1969.
6. Hirschfelder, J.O., Curtiss, C.F., and Bird, R.B., Molecular Theory of Gases and Liquids, John Wiley & Sons, Inc., New York, 1954.
7. Wendt, J.F., "Drag Coefficients of Spheres in Hypersonic Non-Continuum Flow", Final Scientific Report, Contract F61052-69-C-0024, AFCL, 30 November 1971.
8. Kogan, M.N., Rarefied Gas Dynamics, Plenum Press, New York, 1969.
9. Taub, P.A., "Hypersonic, Low Density Sphere and Cone Drag Correlations", AIAA Journal, Vol. 6, No. 8, August 1968, pp. 1577-1579.
10. Geiger, R.E., "Slender-Cone, Zero Angle of Attack Drag in Continuum and Non-Continuum Flow", AIAA Paper No. 69-711, June 1969, AIAA Fluid and Plasma Dynamics Conference, San Francisco, California; also G.E. R68SD15, December 1968.
11. Jones, M.H. and Miller, J.T., "Sharp Cone Measurements in a Rarefied Hypersonic Flow", AIAA Journal, Vol. 7, No. 2, February 1969.
12. Kussoy, M.I., Stewart, D.A. and Hortsman, C.C., "Sharp Slender Cone in Near Free Molecule Hypersonic Flow", AIAA Journal, Vol. 9, No. 9, September 1971.

13. Sims, W.H., "Drag Coefficients of Sharp and Blunt Cones in Highly Rarefied, Supersonic Flow", Rarefied Gas Dynamics, Sixth Symposium, Supplement 5, Academic Press, New York, 1969.
14. Keel, A.G., Jr., Kraize, L.G., PassLore, R.D., and Zapata, R.N., "Hypersonic Low Density Cone Drag", AIAA Paper No. 71-133, Jan. 1971, AIAA 9th Aerospace Sciences Meeting, New York.
15. Smolderen, J.J., Wendt, J.F., Naveau J., and Bramlette, T.T., "Sphere and Cone Drag Coefficients in Hypersonic Transitional Flow", Rarefied Gas Dynamics, Sixth Symposium, Supplement 5, Vol. 1, Academic Press, New York, 1969, pp. 903-907.

TABLE 1

Cone Drag Coefficients - VKI Data

A. Half Angle - 9° (sharp), $T_0 = T_w = 293^\circ\text{K}$
Gas-Air,

| Symbol | $Re_{w,l}$ | $Kn_{\infty,D}$ | $C_D/C_{D_{f.m.}}$ | $C_{D_{f.m.}}$ |
|---|-------------------|-----------------|--------------------|----------------|
|  | 2.97 | 1.20 | 0.820 | 2.34 |
| | 4.22 | 0.850 | 0.795 | |
| | $M_\infty = 6.0$ | 5.24 | 0.684 | |
| | $S_w = 1.75$ | 6.60 | 0.542 | |
| | 7.78 | 0.460 | 0.735 | |
| | 11.1 | 0.322 | 0.685 | |
| | 11.8 | 0.304 | 0.675 | |
| | 13.5 | 0.265 | 0.665 | |
| | 17.4 | 0.206 | 0.615 | |
| | 21.5 | 0.167 | 0.580 | |
| | 25.3 | 0.141 | 0.390 | |
| | 31.4 | 0.114 | 0.365 | |
| | 41.6 | 0.0860 | 0.340 | |
| | 52.2 | 0.0685 | 0.320 | |
|  | 3.84 | 0.725 | 0.975 | 2.22 |
| | 4.94 | 0.564 | 0.920 | |
| | $M_\infty = 8.1$ | 6.05 | 0.460 | |
| | $S_w = 1.80$ | 7.15 | 0.388 | |
| | 8.85 | 0.314 | 0.850 | |
| | 11.6 | 0.239 | 0.790 | |
| | 14.7 | 0.189 | 0.755 | |
| | | | | |
|  | 3.03 | 0.916 | 1.04 | 2.22 |
| | 3.78 | 0.736 | 1.02 | |
| | $M_\infty = 8.1$ | 4.87 | 0.571 | |
| | $S_w = 1.80$ | 5.84 | 0.476 | |
| | 8.82 | 0.315 | 0.920 | |
| | 11.6 | 0.240 | 0.850 | |
| | 14.7 | 0.189 | 0.820 | |
| | | | | |
|  | 1.78 | 1.28 | 1.02 | 2.19 |
| | 2.07 | 1.10 | 0.990 | |
| | $M_\infty = 10.4$ | 3.42 | 0.665 | |
| | $S_w = 1.83$ | 4.31 | 0.527 | |
| | | | | |
|  | 1.84 | 1.23 | 1.01 | 2.19 |
| | 2.36 | 0.963 | 0.925 | |
| | $M_\infty = 10.4$ | 3.25 | 0.698 | |
| | $S_w = 1.83$ | 4.25 | 0.535 | |
| | | | | |

B. Half Angle - 13.5° (sharp), $T_0 = T_w = 293^\circ\text{K}$



| Symbol | $Re_{w,l}$ | $Kn_{\infty,D}$ | $C_D/C_{D_{f.m.}}$ | $C_{D_{f.m.}}$ |
|---|------------|-----------------|--------------------|----------------|
|  | 2.39 | 0.808 | 0.965 | 2.25 |
| | 2.42 | 0.798 | 0.975 | |
| $M_\infty = 8.1$ | 3.12 | 0.619 | 0.940 | |
| $S_w = 1.80$ | 3.77 | 0.511 | 0.915 | |
| Nitrogen | 5.25 | 0.368 | 0.875 | |
| | 5.26 | 0.367 | 0.890 | |
| | 7.65 | 0.252 | 0.805 | |
| | 11.6 | 0.166 | 0.720 | |
| | 18.5 | 0.104 | 0.655 | |
|  | 3.92 | 0.231 | 0.960 | 2.27 |
| | 5.13 | 0.177 | 0.900 | |
| $M_\infty = 11.5$ | 5.85 | 0.155 | 0.875 | |
| $S_w = 1.56$ | 6.60 | 0.137 | 0.850 | |
| Argon | 6.71 | 0.135 | 0.835 | |
| | 7.31 | 0.124 | 0.825 | |
| | 8.13 | 0.111 | 0.790 | |
| | 9.62 | 0.0943 | 0.760 | |
| | 13.0 | 0.0695 | 0.700 | |
| | 18.9 | 0.0480 | 0.605 | |
| | 18.9 | 0.0480 | 0.595 | |
| | 34.1 | 0.0266 | 0.470 | |
| | 35.8 | 0.0253 | 0.450 | |
| | 51.9 | 0.0175 | 0.395 | |

TABLE 2

Experimental Conditions for Data Presented

| Symbol | S_w | M_∞ | θ_c | Gas | Ref |
|--------|-------|------------|------------|----------------|---------|
| \pm | 1.75 | 6.0 | 9° | Air | Present |
| X | 1.80 | 8.1 | 9° | Air | " |
| + | 1.80 | 8.1 | 9° | Air | " |
| □ | 1.83 | 10.4 | 9° | Air | " |
| ■ | 1.83 | 10.4 | 9° | Air | " |
| ▽ | 1.80 | 8.1 | 13.5° | Nitrogen | 15 |
| △ | 1.56 | 11.5 | 13.5° | Argon | 15 |
| □ | 10.1 | 24.3 | 5° | Air | 12 |
| □ | 10.1 | 24.3 | 10° | Air | 12 |
| ● | 6.06 | 10 | 15° | Nitrogen | 11 |
| ● | 4.28 | 9.4 | 15° | Nitrogen | 11 |
| △ | 5.0 | 24.2 | 6° | Nitrogen | 10 |
| △ | 5.0 | 24.2 | 15° | Nitrogen | 10 |
| ○ | 1.80 | 7.64 | 9° | Nitrogen | 14 |
| ○ | 1.63 | 3.7 | 10° | Carbon dioxide | 13 |

All cones were listed as "sharp" ($R_n/R_b \leq 0.05$).

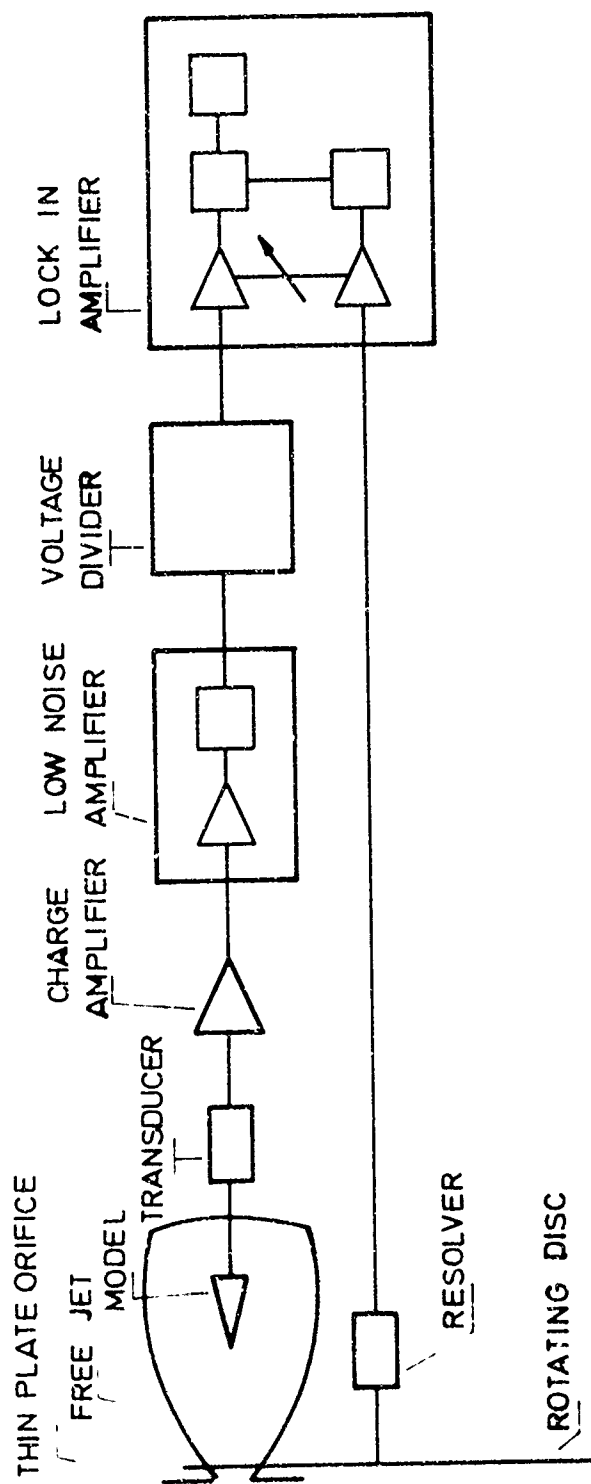


FIGURE 1 - BLOCK DIAGRAM OF MODULATED FLOW SYSTEM

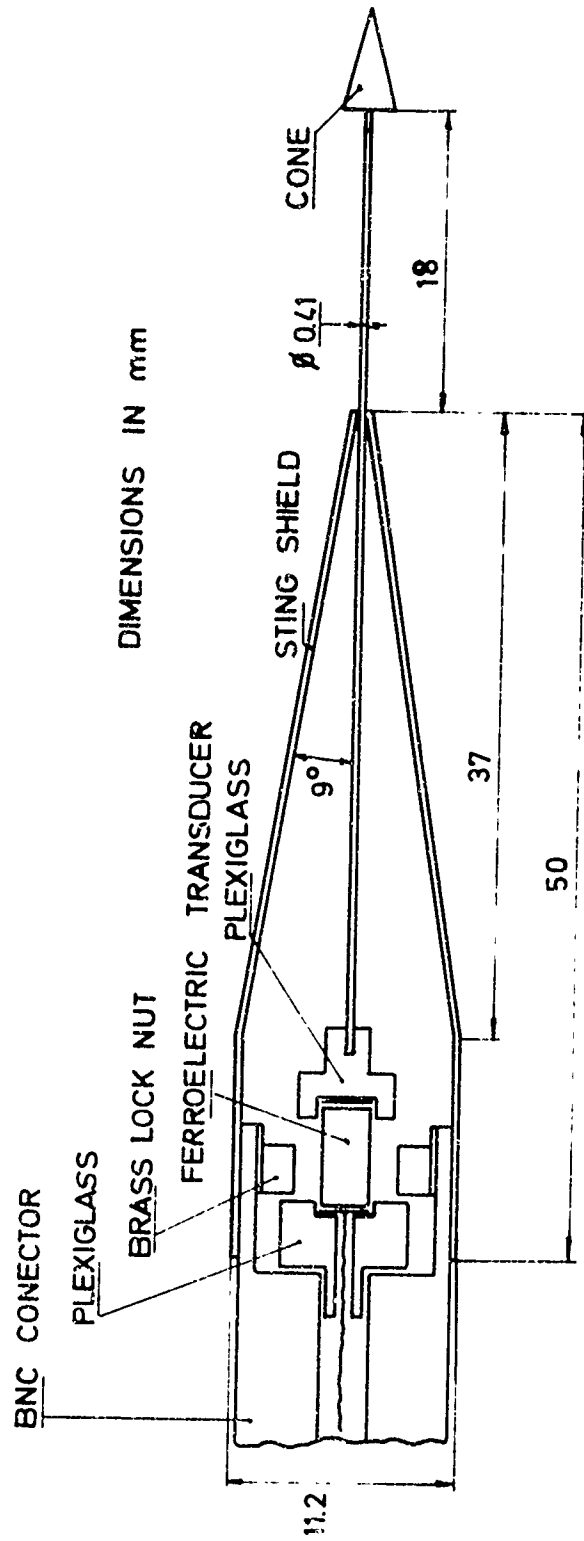


FIGURE 2 - SCHEMATIC OF FORCE PROBE

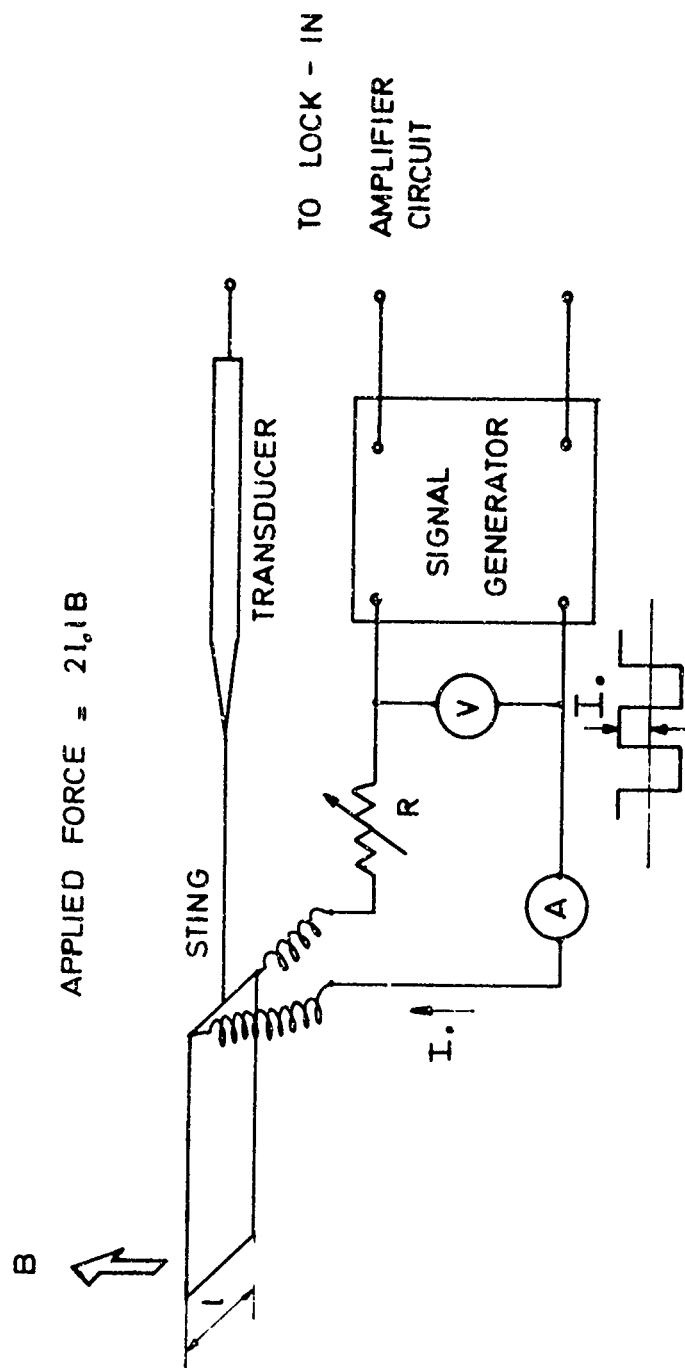


Fig 3 SCHEMATIC OF CALIBRATION ARRANGEMENT

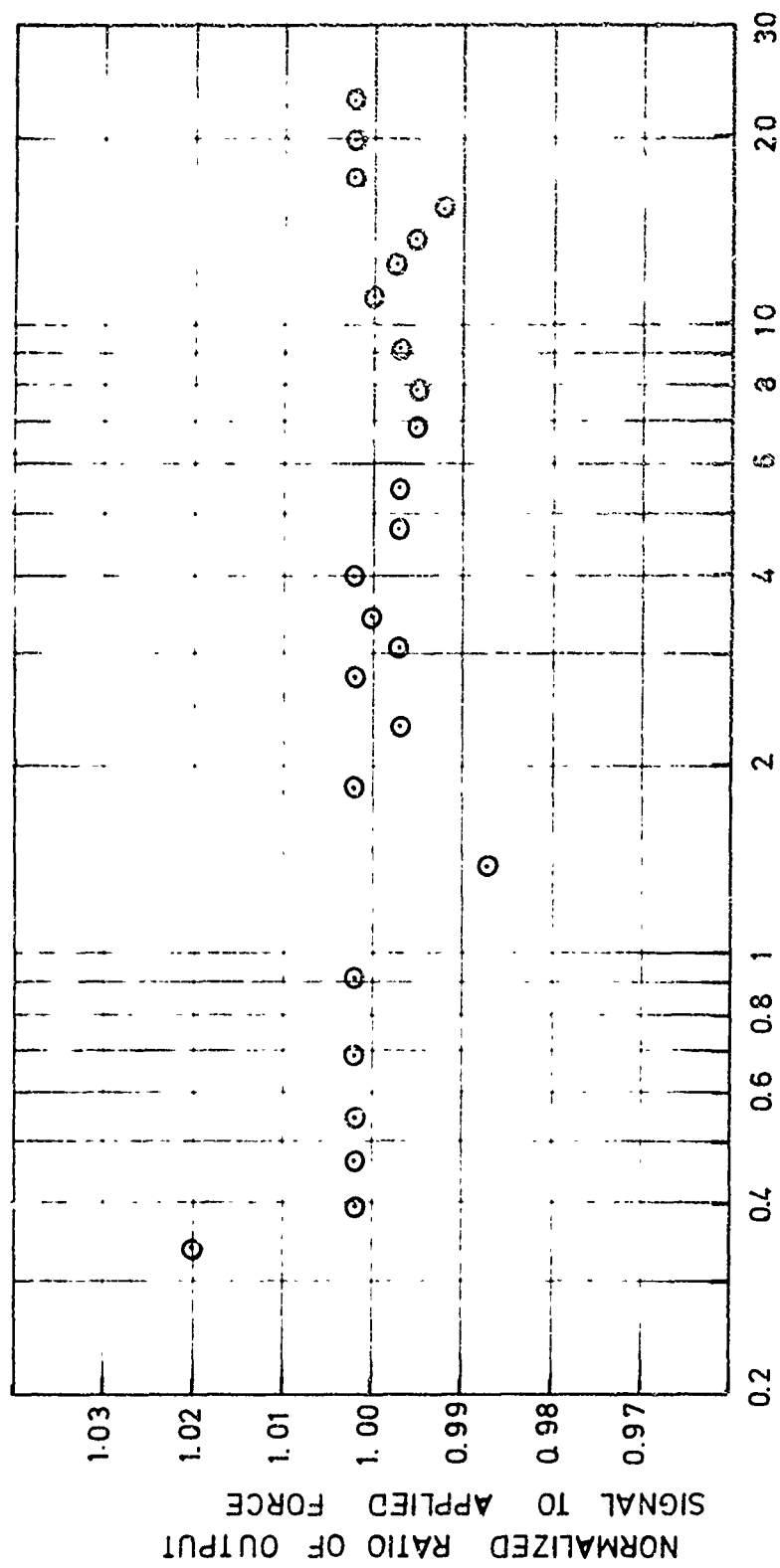
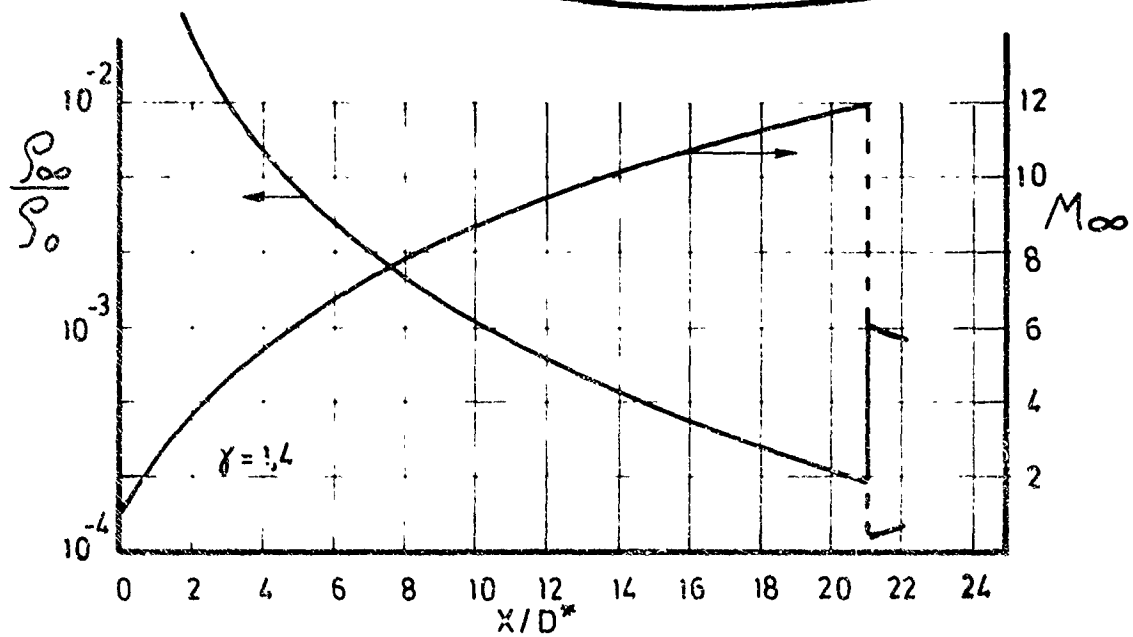
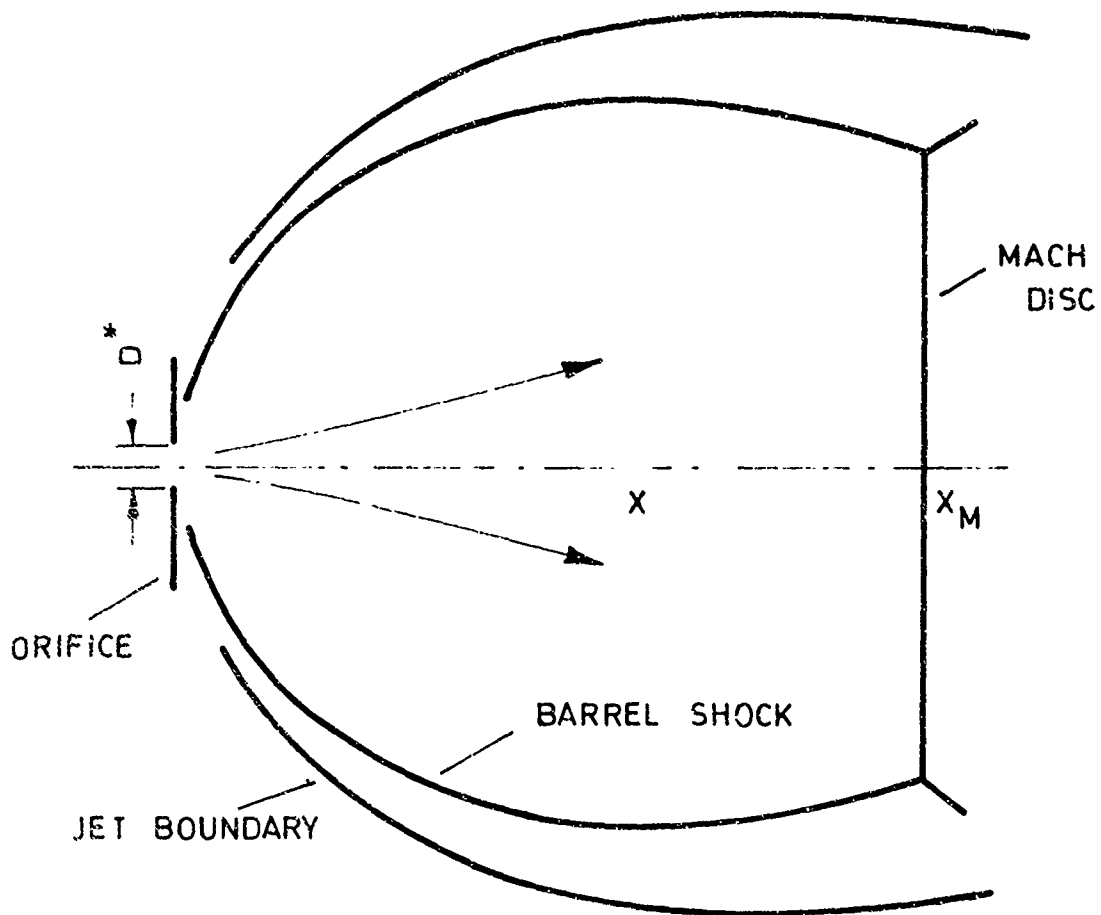


FIGURE 4. TYPICAL TRANSDUCER CALIBRATION



CHARACTERISTICS OF FREE JET
EXPANSION FOR HYPERSONIC FLOW
FIGURE 5

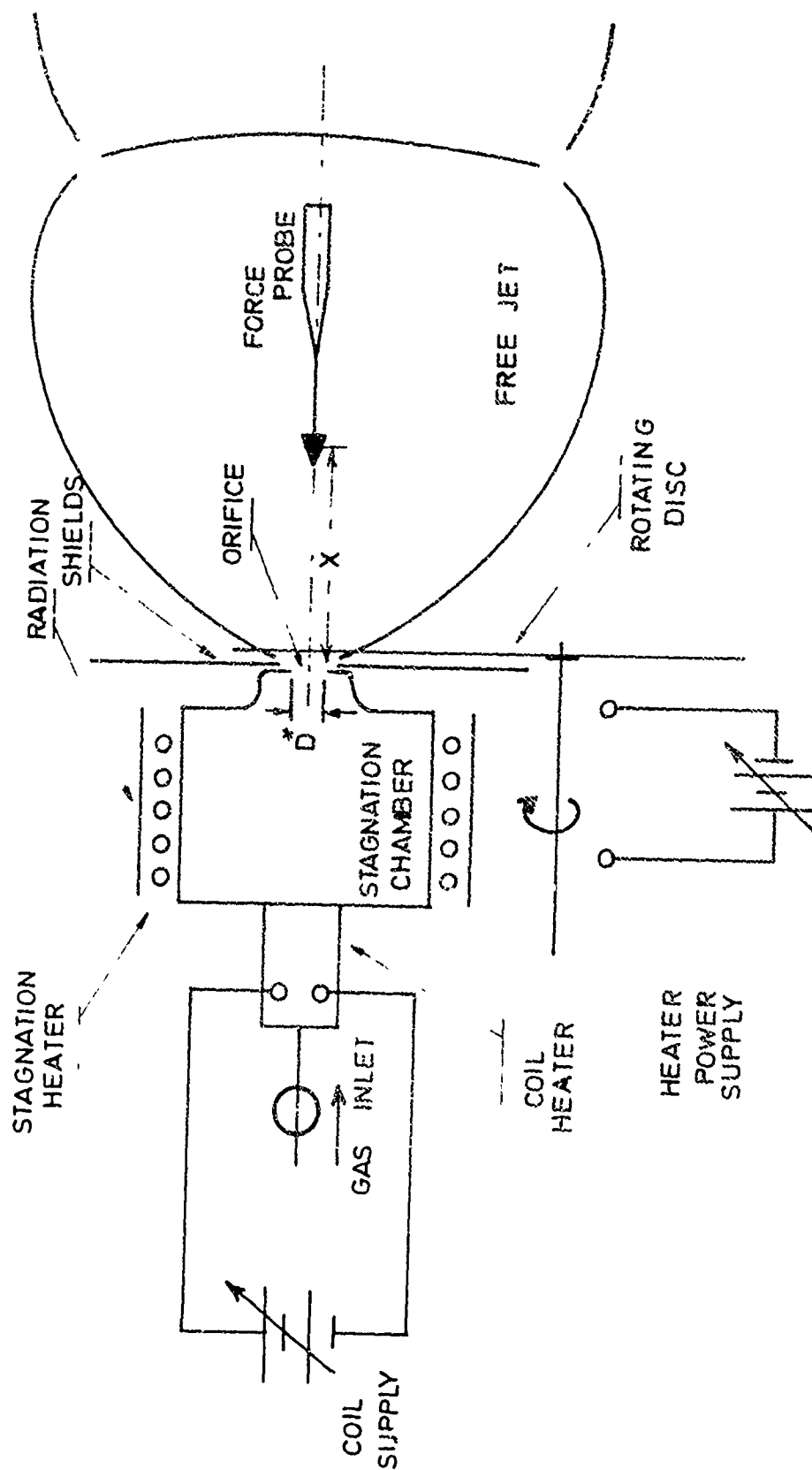


FIGURE 6 -SCHEMATIC OF INCONEL HEATER

HOT WIRE SIGNAL

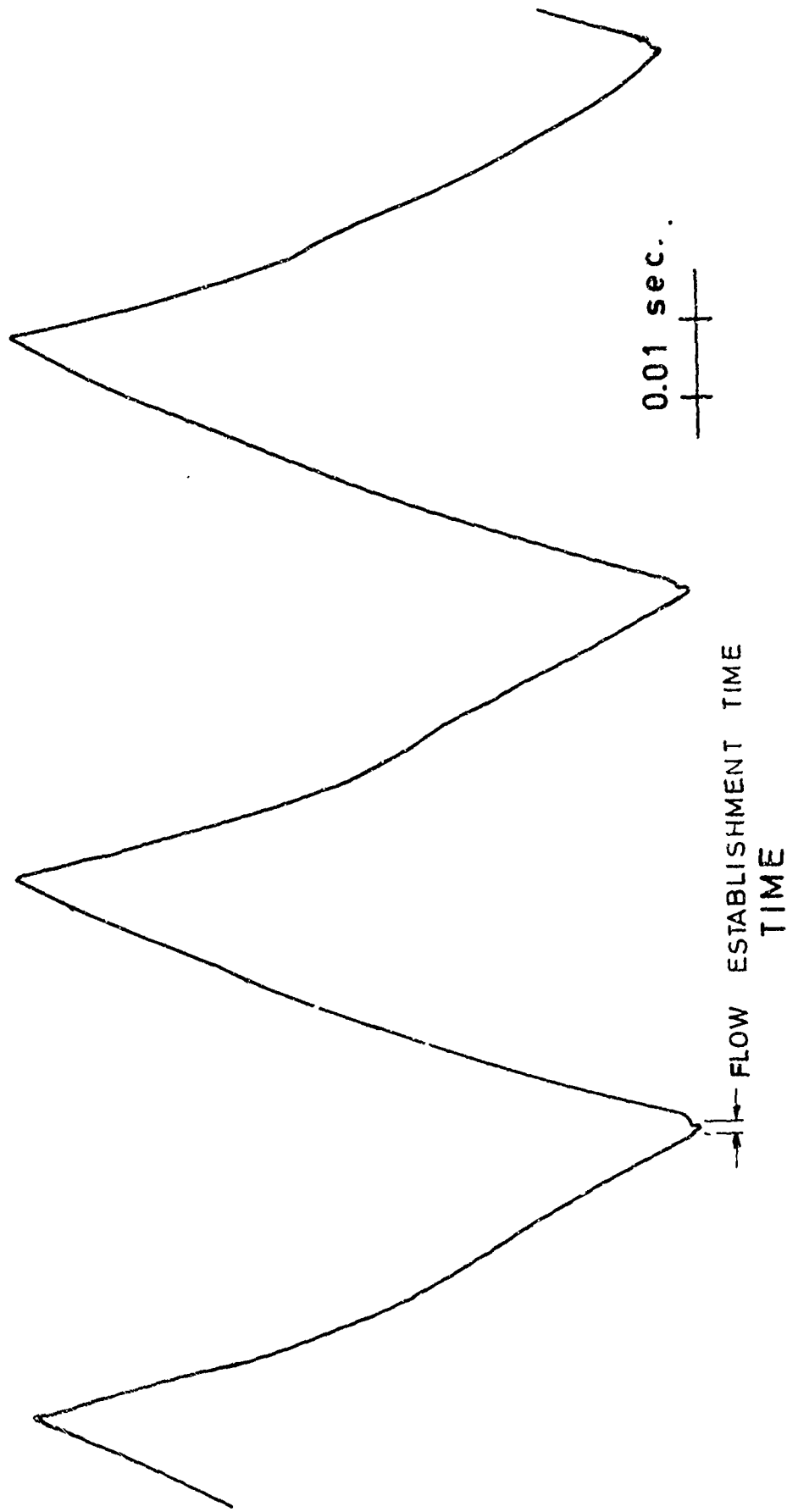


FIGURE-7 FLOW ESTABLISHMENT IN A MODULATED FREE JET

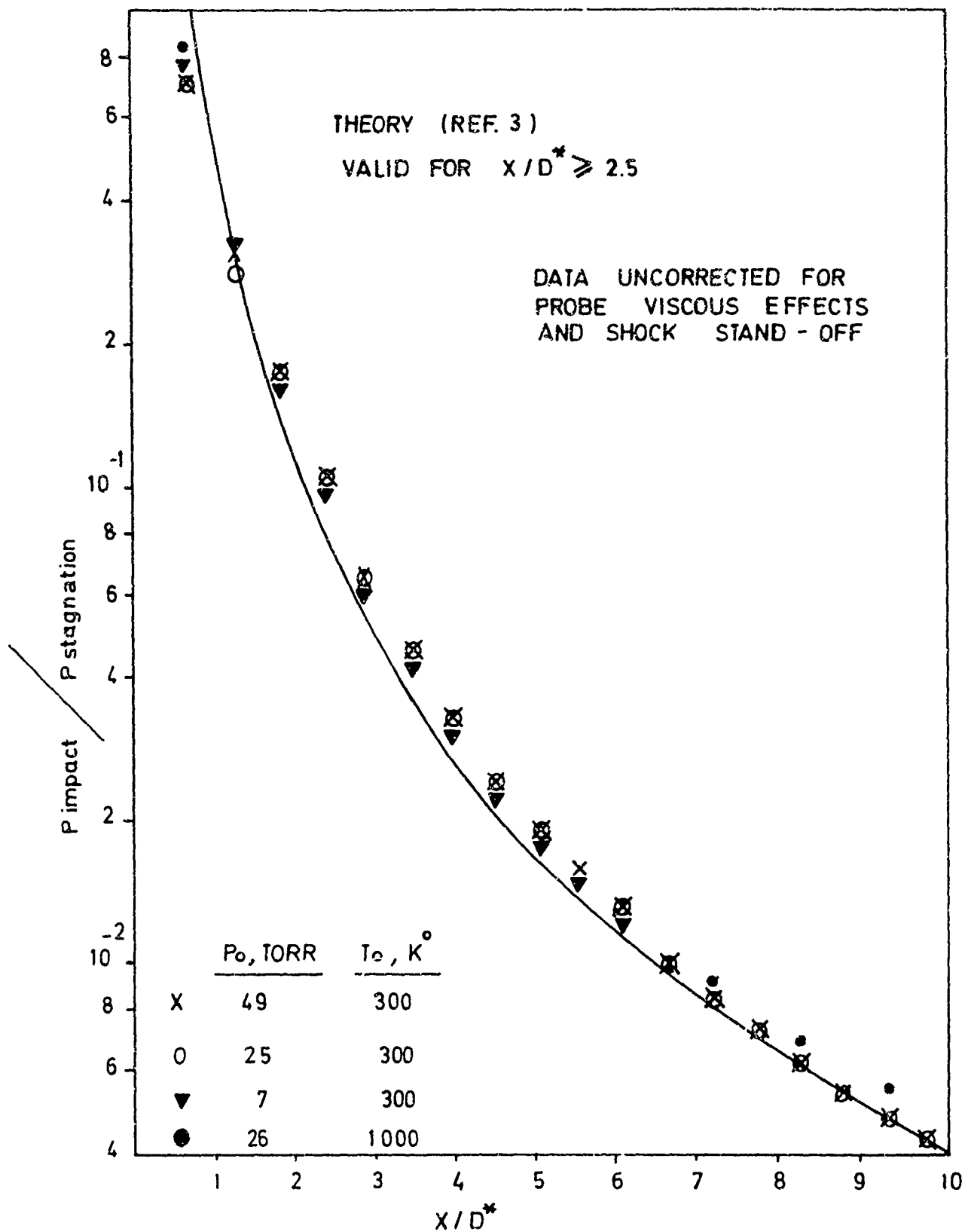
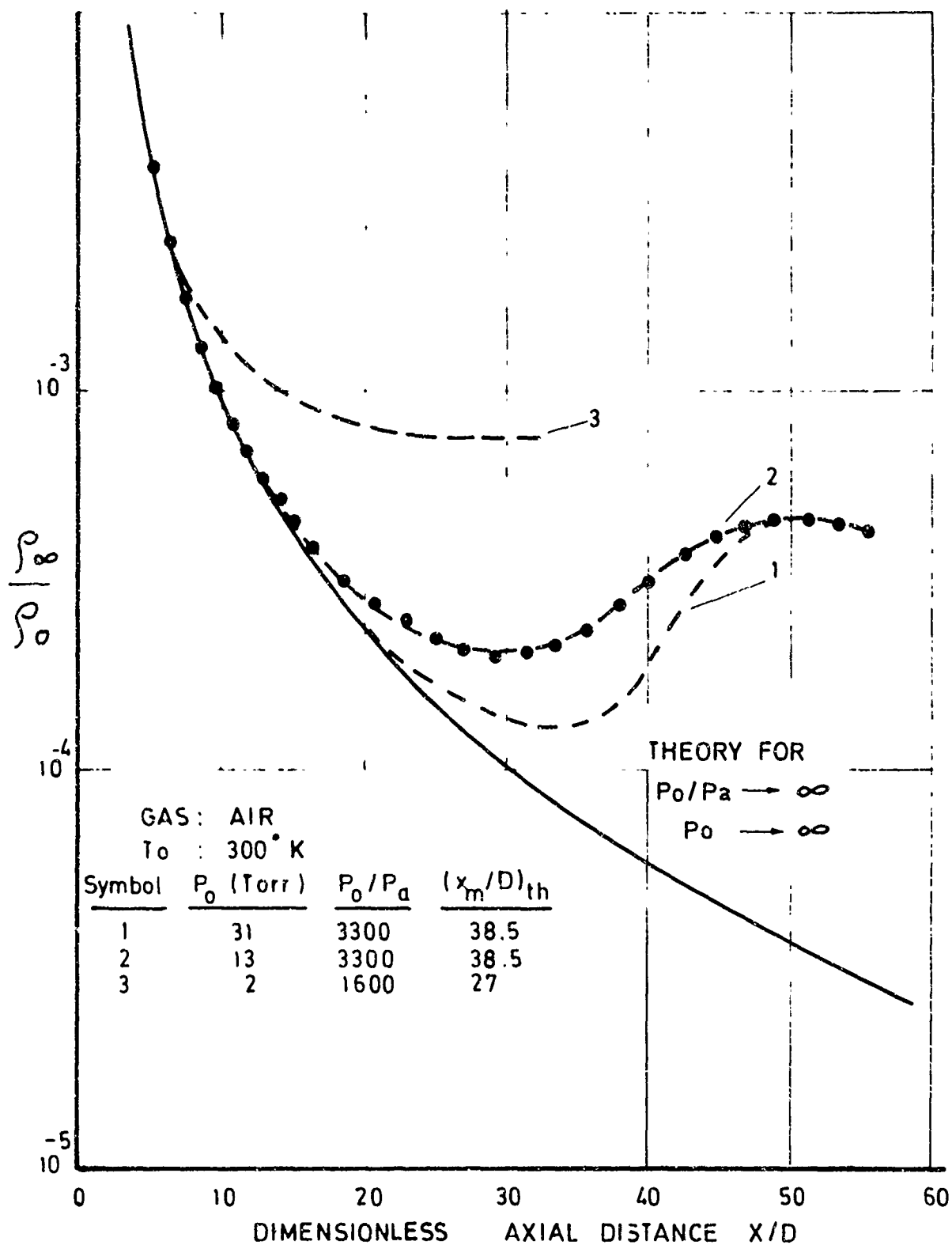
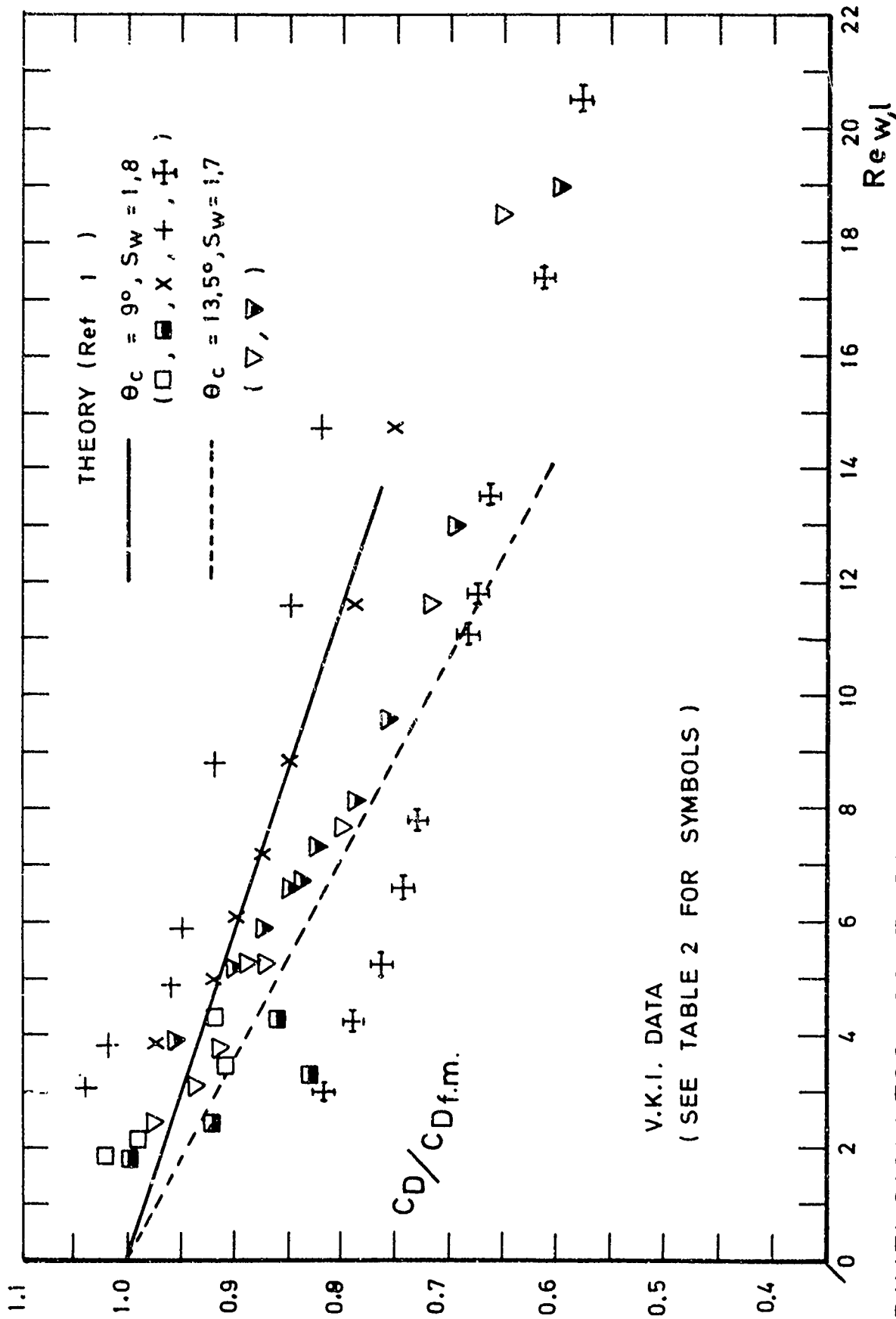


Fig.8 IMPACT PRESSURE VARIATION IN FREE JET



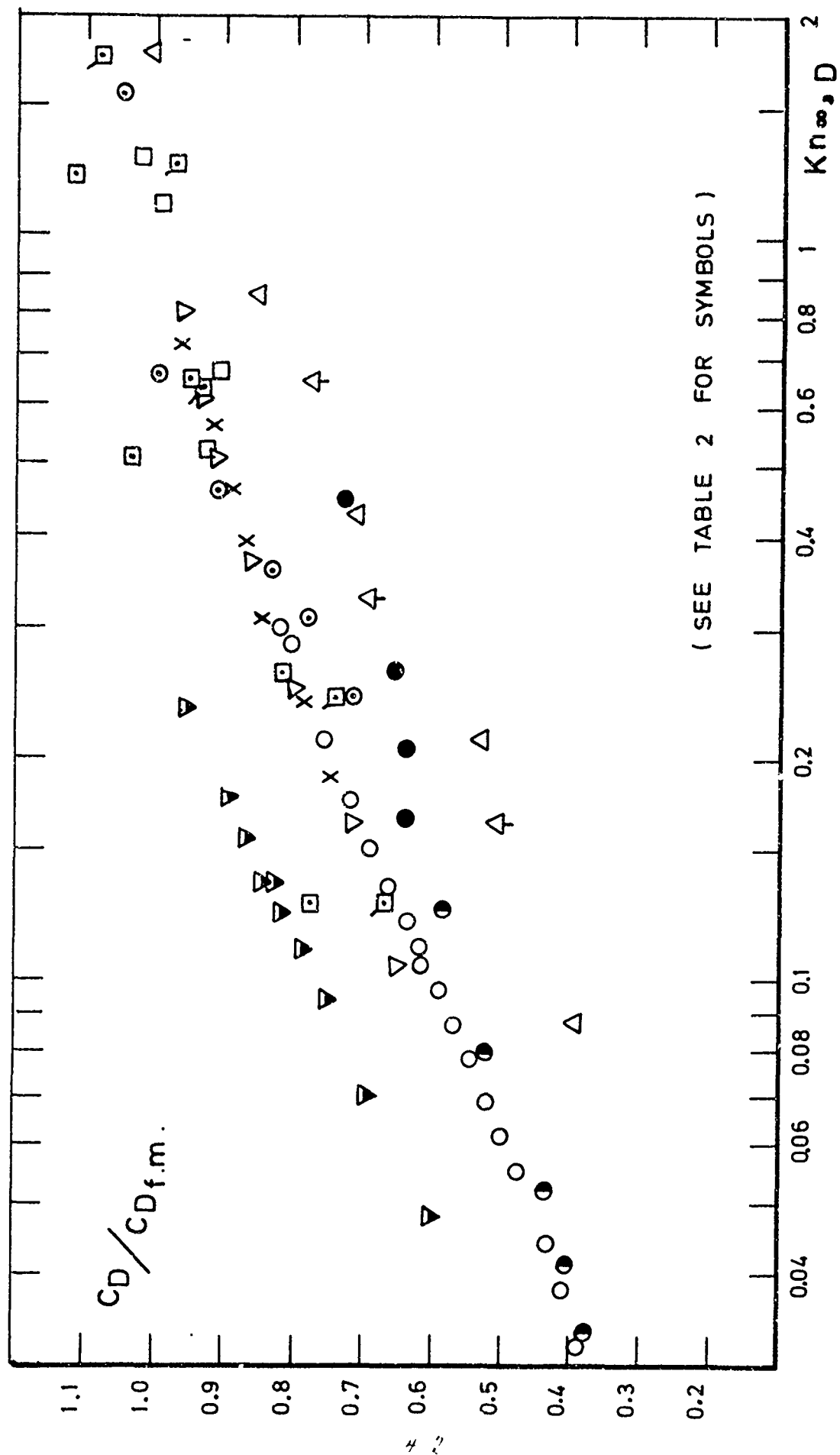
DENSITY VARIATION ON FREE JET
 CENTERLINE MEASURED WITH ELECTRON
 BEAM FLOURESCENCE PROBE

FIGURE-9



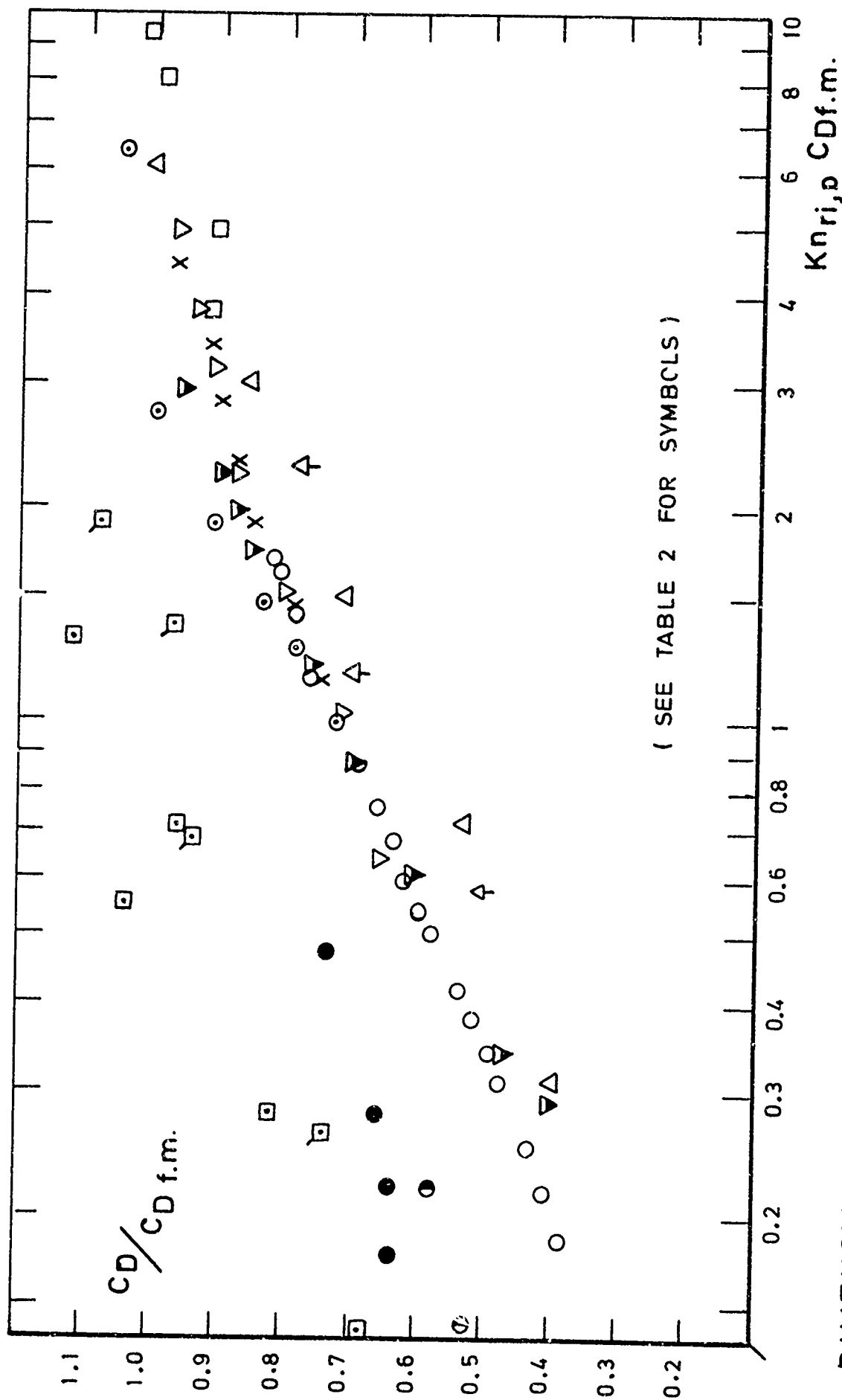
DIMENSIONLESS CONE DRAG COEFFICIENT VS WALL REYNOLDS NUMBER

FIGURE - 10

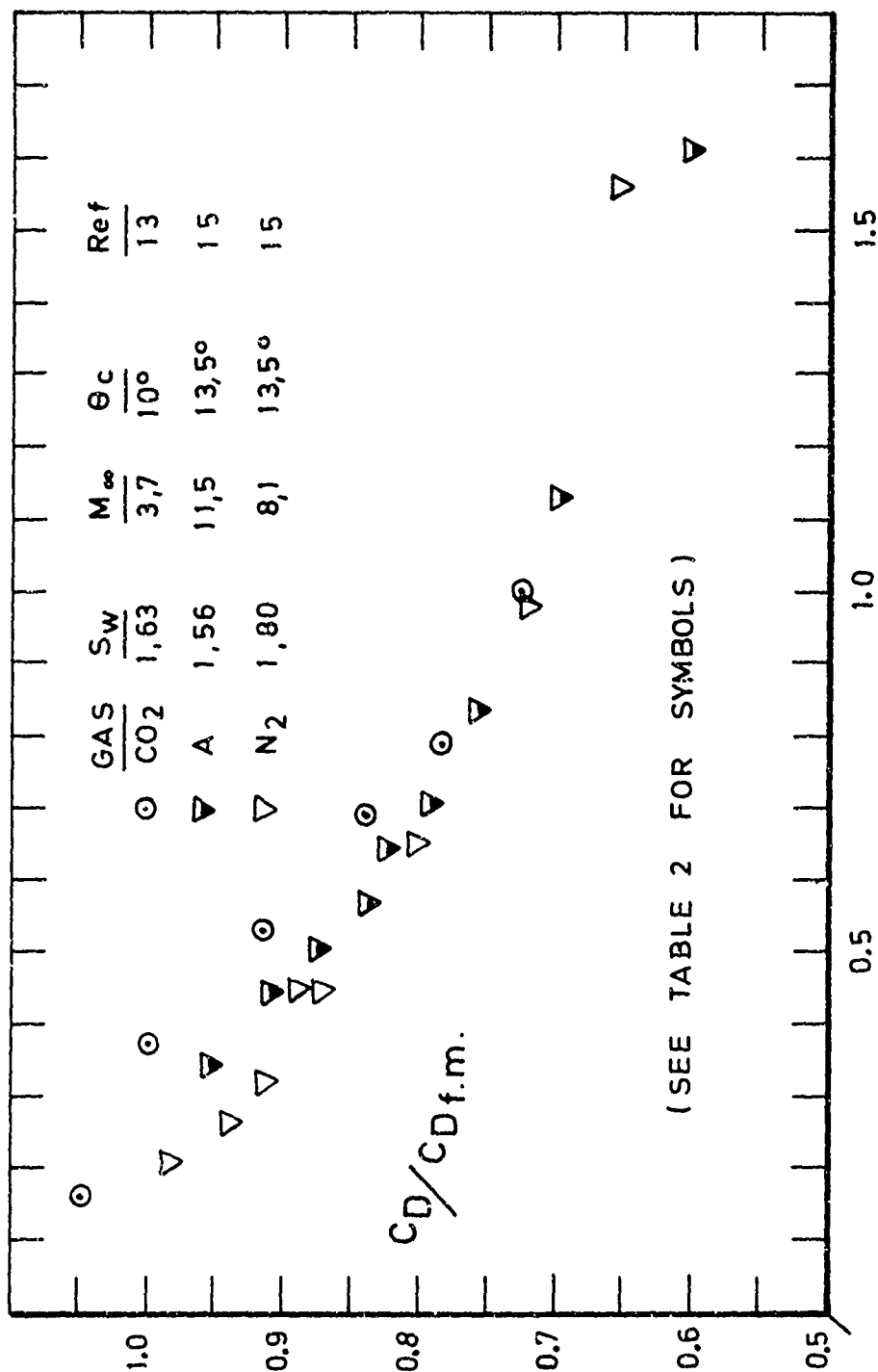


DIMENSIONLESS CONE DRAG COEFFICIENT VERSUS KNUDSEN NUMBER

FIGURE - 11



DIMENSIONLESS CONE DRAG COEFFICIENT VS EFFECTIVE KNUDSEN NUMBER
FIGURE-12



DIMENSIONLESS CONE DRAG COEFFICIENT FOR VARIOUS GASES

FIGURE-13